

2D-numerical analysis of hydraulic fracturing in heterogeneous geo-materials

S.Y. Wang^{a,*}, L. Sun^{b,c,1}, A.S.K. Au^{d,2}, T.H. Yang^{e,3}, C.A. Tang^{f,4}

^a Center for Geotechnical and Materials Modelling, University of Newcastle, University Drive, Callaghan, NSW 2238, Australia

^b Transportation College, Southeast University, Nanjing 210096, China

^c Department of Civil Engineering, Catholic University of America, Washington, DC 20064, USA

^d Department of Civil Engineering, The University of Hong Kong, Pokfulam Road, Hong Kong

^e Centre for Rock Instability and Seismicity Research, Northeastern University, Shenyang 110004, PR China

^f School of Civil and Hydraulic Engineering, Dalian University of Technology, Dalian 116024, PR China

ARTICLE INFO

Article history:

Received 14 July 2008

Received in revised form 1 December 2008

Accepted 1 December 2008

Available online 22 January 2009

Keywords:

Hydraulic fracture
Numerical simulation
Cavity expansion
Stiff soil
Heterogeneity

ABSTRACT

A geo-material failure process analysis (F-RFPA2D), considering the coupling of stress distribution, fluid flow, and element damage evolution, is used to investigate the mechanisms of crack initiation and propagation around a 2-D cylindrical cavity in heterogeneous stiff soils during hydraulic fracturing. A large number of numerical analysis on hydraulic fracturing in stiff soil with pre-existing injection cavity have been carried out to study the mechanism of hydraulic fracturing in stiff soil. In addition, the characteristic of acoustic emission (AE) due to hydraulic fractures are studied by numerical simulations. The results provide a better understanding of the crack initiation and propagation mechanisms during hydrofracturing. The simulation software package can be a powerful tool for study of soil behavior during hydraulic fractures.

Crown Copyright © 2008 Published by Elsevier Ltd. All rights reserved.

1. Introduction

Hydraulic fracturing is a common technique used in petroleum engineering, mining engineering and grouting engineering for many years. Hydraulic fractures are created in the vicinity of a borehole when fluid is injected at a pressure that exceeded some critical value. Hydraulic fractures created during permeation or compaction grouting can affect the distribution of grout and markedly reduce the ability of grout to seal or increase strength [1,2]. Since Hubbert and Willis [3] developed the first realistic model relating the recorded hydraulic fracturing test variables to the in situ state of stress in rock, hydraulic fracturing had been first applied to the determination of in situ stresses in soil, and its importance in geotechnical engineering had also been paid much more attention than ever.

Much attention have been paid to the mechanism of hydraulic fracturing in soil, which had also been gradually recognized in connection with pressure grouting [4–9]. Bjerrum and Anderson [10]

investigated the in situ measurement of lateral pressure in clay and demonstrated by theoretical analysis of the problem. Bjerrum et al. [11] also performed in situ outflow permeability tests in ground to evaluate the effect of hydraulic fracturing in soils. Hassani et al. [12] observed the vertical pattern of cracks for all the specimens tested during hydraulic fracturing around a borehole, but the lateral pressure coefficient K_0 or other related parameters of the specimens in his tests were not specified.

In a saturated cohesive soil, it is very useful to determine the influence zone around cavity and the generation and the dissipation of pore water pressure during and after cavity expansion. The usual procedure for analytical analysis (cavity expansion theory) is described as follows: in Fig. 1, r_0 is the initial radius, r_p is the plastic radius, p_1 is the injecting pressure, σ_r and σ_θ are normal stresses acting in the radial and tangential directions respectively; p is pore water pressure. Based on the geometry equation, constitutive equation, equilibrium equation and some yield criteria, such as Mohr–Coulomb criteria, the plastic zone radius, radial stress at elastoplastic interface and pore pressure can be determined. This analytical method have gained many successes in applications in study the behavior of geo-materials during pressure meter test, cone penetration test, pile driving, compaction grouting, cratering by explosives, tunneling, etc. [13–17]. However, due to the complicated material properties and boundaries, these analytical methods have two major limitations. Firstly, because of the heterogeneity and anisotropic of the soils, the fractures can occur around the cavity due to the hydraulic pressure. The fractures will

* Corresponding author. Tel./fax: +61 249216082.

E-mail addresses: bcwangsy@126.com (S.Y. Wang), sunl@cua.edu (L. Sun), skau@hkucc.hku.hk (A.S.K. Au), yangtianhong@mail.neu.edu.cn (T.H. Yang), catang@mechsoft.cn (C.A. Tang).

¹ Tel.: +1 202 3196671; fax: +1 202 3196677.

² Tel.: +852 28578552; fax: +852 25595337.

³ Tel./fax: +86 024 83687705.

⁴ Tel./fax: +86 0411 87403588.

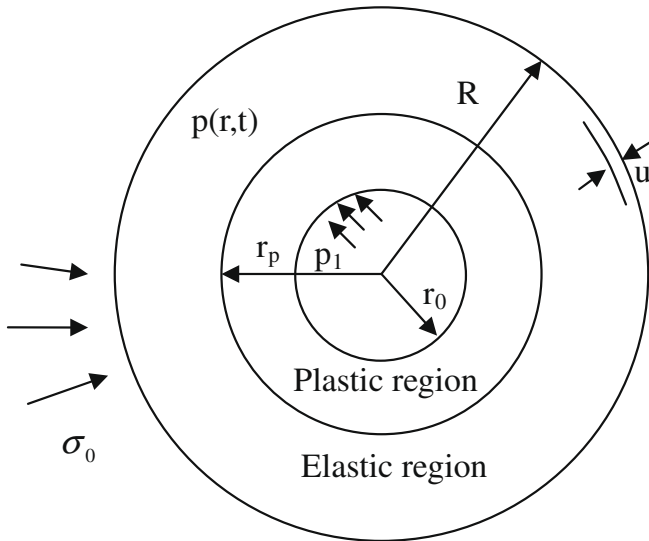


Fig. 1. Cavity under uniform internal and external pressures.

propagate and interact with each other. Meanwhile, for the different K_0 conditions, the stress field will influence the hydraulic fractures propagation. That is the coupling effect of seepage, damage and stress field, which is difficult for the cavity expansion theory to analyze. Secondly, geotechnical engineer designing a grouting process always faces the critical questions: (1) when will soil fractures occur, i.e. at what injection pressure? and (2) how will the resulting fractures propagate? To answer these questions, one need to understand the fundamental mechanism of fracture initiation and the subsequent fracture propagation. The investigations described in this paper are performed: (1) to develop a better fundamental understanding of the crack initiation mechanism of hydrofracturing by injection pressure in stiff soil and (2) to better understand the propagation of cracks afterwards.

In this paper, a numerical model that can consider the coupling effect of seepage, damage and stress field is introduced. Two-dimensional numerical simulations of the behavior of cylindrical cavity in the center of a saturated stiff soil subjected to different initial in situ stresses and an increasing injection pressure are performed to examine the initiation of tensile cracks and/or shear cracks and their subsequent propagation. The characteristics of acoustic emission (AE) due to hydraulic fractures are simulated. Moreover, the influence of heterogeneity of stiff soil on hydraulic fractures is studied by numerical tests.

2. Mechanics of fracture initiation and propagation

Traditionally, crack initiation in geo-materials is considered to be either a tensile failure or shear failure in the material. Some researchers [5,18] considered hydraulic fracture was initiated by a shear failure, while others [19,20], considered it was initiated by a tensile failure. Assuming hydraulic fracturing is the formation of a tensile fracture through soil, the empirical total stress equation developed by Jaworski et al. [4] have been used to determine the hydraulic fracturing pressure as a function of in situ stress and tensile strength of the soil

$$P_f = n\sigma_{3i} + \sigma_t \quad (1)$$

where P_f is hydraulic fracturing pressure; n is an empirical factor depending on the stress redistribution around a borehole and the total stress path for the soil, ranging from 1.5 to 1.8; σ_{3i} is initial minor total principal stress in the soil and σ_t is total tensile strength of the soil.

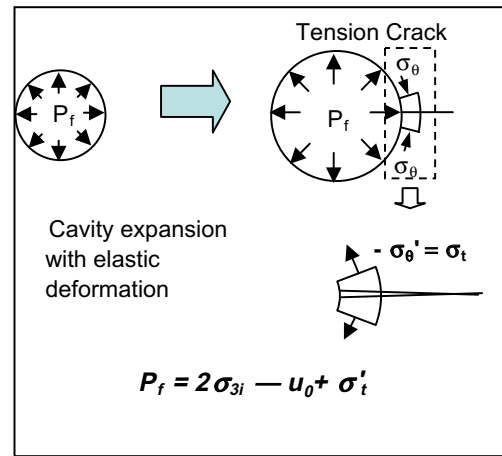


Fig. 2. Tensile Fracture Mechanisms [34].

On the basis of cylindrical cavity expansion analyses, Soga et al. [21] developed the tensile failure and shear failure mechanisms as shown in Figs. 2 and 3, respectively. For tensile failure, the relationships between hydraulic fracturing pressure and tensile strength of the soil were

$$P_f = 2\sigma_{3i} - 2u_0 + \sigma_t \quad (\text{in terms of total stress}) \quad (2)$$

$$P_f = 2\sigma_{3i} + u_0 + \sigma'_t \quad (\text{in terms of effective stress}) \quad (3)$$

where u_0 is the initial pore water pressure and σ'_t is the effective tensile strength of soil. The equation is identical to that developed by Andersen et al. [8] using elasticity theory. It can be observed that the hydraulic fracturing pressure increases linearly with initial confining pressure with a slope of two for tension induced soil fracture.

Soil is assumed to be an elastic material in the derivation of Eqs. (2 and 3). As a result, the increase in radial stress causes an equivalent reduction in circumference stress. However, the assumption may not be true in reality as the stress–strain behavior of soil was highly non-linear. Alfaro and Wong [22] demonstrated that the stress conditions around an injection well during grouting did not follow a linear elastic stress path.

Before the circumferential effective stress diminished for soils of no tensile strength or reaches the tensile strength for cemented soils, shear failure can occur in soil when the stress conditions satisfied the Mohr–Coulomb shear failure criterion as shown in Fig. 2. Using the failure criteria of undrained shear strength

$$(\sigma_r - \sigma_\theta) = 2S_u \quad (4)$$

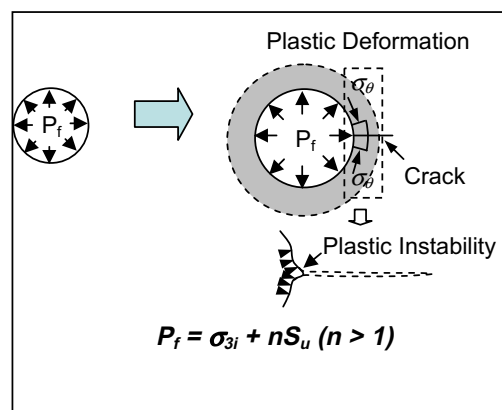


Fig. 3. Shear Fracture Mechanisms [34].

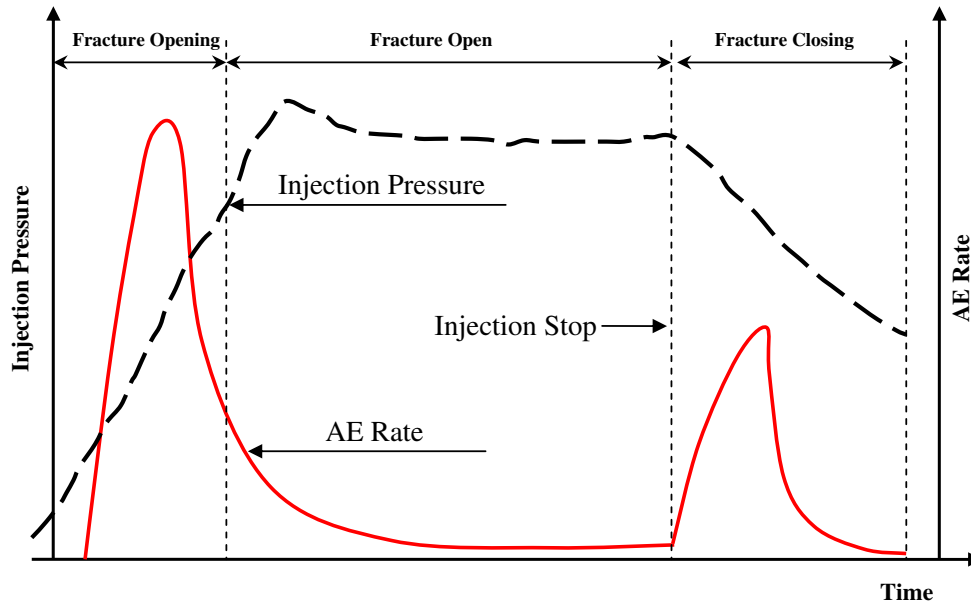


Fig. 4. Typical AE signatures for hydraulic fracturing test.

where σ_r is total radial stress; σ_θ is total circumferential stress and S_u is undrained shear strength, Soga et al. [21] derived a relationship between hydraulic fracturing pressure and undrained shear strength of soil for shear failure

$$P_f = \sigma_{3i} + nS_u \quad (\text{in terms of total stress}) \quad (5)$$

$$P_f = \sigma'_{3i} + u_0 + nS_u \quad (\text{in terms of effective stress}) \quad (6)$$

where n is a constant depending on the radius of the cavity and the radius of the plastic zone. It can be observed that the hydraulic fracturing pressure is a linear function of the initial confining pressure with a unit slope for shear induced soil fracture. It should be noted that the criteria mentioned above is just to determine whether the fracture will initiate. However, the fracture propagation mechanisms are still undetermined. In order to explore this mechanism, finite element analysis are carried out in the following sections.

3. Numerical model

3.1. Brief description of numerical model

The model, developed by Tang et al. [23], is a numerical simulation tool using finite element analyses to handle progressive failure of heterogeneous and permeable geo-materials. Coupled seepage and stress variations in saturated geological media are described by Biot's theory of consolidation. Having included stress effects on permeability, the basic formulations of the analysis are

$$\text{Equilibrium equation: } \frac{\partial \sigma_{ij}}{\partial x_j} + \rho X_j = 0 \quad (i, j = 1, 2, 3) \quad (7)$$

Strain–displacement equation :

$$\varepsilon_{ij} = \frac{1}{2}(u_{ij} + u_{j,i}) \quad \varepsilon_v = \varepsilon_{11} + \varepsilon_{22} + \varepsilon_{33} \quad (8)$$

$$\text{Constitutive equation: } \sigma'_{ij} = \sigma_{ij} - \alpha p \delta_{ij} = \lambda \delta_{ij} \varepsilon_v + 2G \varepsilon_{ij} \quad (9)$$

$$\text{Seepage equation: } k \nabla^2 p = \frac{1}{Q} \frac{\partial p}{\partial t} - \alpha \frac{\partial \varepsilon_v}{\partial t} \quad (10)$$

$$\text{Coupling equation: } k(\sigma, p) = \xi k_0 e^{-\beta(\frac{\sigma_{ij}}{3} - \alpha p)} \quad (11)$$

where σ = stress; ρ = unit weight of soil; ε = strain; α = coefficient of pore water pressure; p = pore water pressure; λ = Lamé coefficient; δ = Kronecher constant; G = modulus of shear deformation; Q = Biot's constant; k = coefficient of permeability; k_0 = reference coefficient of permeability; β = coupling parameter that reflects the influence of stress on the coefficient of permeability and ξ (>1) = damage factor to accounts for the increase of permeability of the material during fracture formation. Eqs. (7)–(10) are derived

Table 1
Input material properties parameters for numerical models.

Index	Value
Homogeneity index, m	1.5, 3, 5, 8, 15
Coefficient of lateral earth pressure, K_0	0.3, 0.5, 0.8, 1, 1.2, 1.5, 2
Young's modulus, E_0	5000 kPa
Effective stress cohesion intercept, C'	30 kPa
Internal friction angle, ϕ'	30°
Poisson's ratio, ν	0.25
Coefficient of residual strength, η	0.8
Coefficient of permeability, k_0	2×10^{-9} m/s
Incremental injection pressure, ΔP	1 kPa

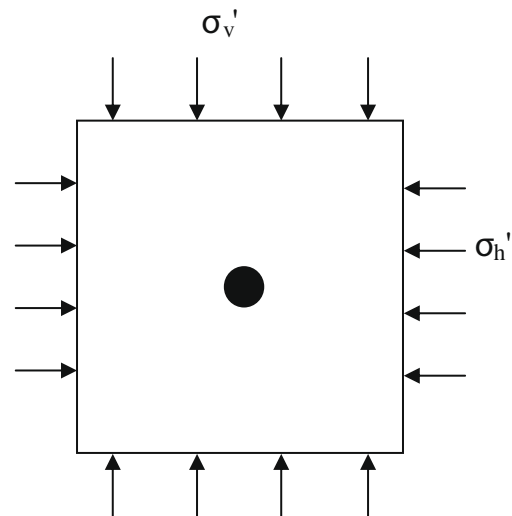


Fig. 5. Numerical model.

from Biot’s theory of consolidation. Eq. (11) is introduced to describe the dependency of permeability on stress and damage. The relationship between permeability and stress is assumed to follow a negative exponential function. For heterogeneity of geo-materials, the material properties for different elements are randomly distributed throughout the domain of analysis following a Weibull distribution:

$$\varphi = \frac{m}{\mu_0} \left(\frac{\mu}{\mu_0}\right)^{m-1} \exp \left[-\left(\frac{\mu}{\mu_0}\right)^m\right] \quad (12)$$

where μ = material property variable; μ_0 = mean value of the corresponding material property; m = homogeneity index, i.e., a parameter defined the shape of the distribution function that defined the degree of material heterogeneity, a larger m implied a more homogeneous material and vice versa. Therefore, the parameter m is called the homogeneity index in RFPA^{2D}. For higher values of the homogeneity index, the strengths of more elements are concentrated closer to μ_0 .

In addition, both tensile and shear failures are considered in the analysis. An element is considered to have failed in the tension mode when its minor principal stress exceeds the tensile strength of the element (Eq. (13)), and to have failed in the shear mode when the shear stress satisfied the Mohr–Coulomb failure criterion (Eq. (14))

$$F = (C' + \sigma' \tan \phi') - \tau \quad (13)$$

$$\sigma'_3 \leq -\sigma'_t \quad (14)$$

where was τ the shear stress, σ' was the effective normal stress, C' the effective stress cohesion intercept, ϕ' the effective stress angle of friction or shearing resistance, σ'_3 the minor effective principal stress and σ'_t the tensile failure strength of the element.

For an individual element, when the stress of the element satisfied the certain strength criterion, the element begins to damage. Karihaloo and Fu [24] have used a damage-based constitutive law to study the plain concrete tension. According to isotropic elastic damage theory, the elastic modulus of element may degrade gradually as damage progresses, and the elastic modulus of damaged material can be defined as follows:

$$E = (1 - D)E_0 \quad (15)$$

where D is the damage variable and E and E_0 are elastic modulus of the damaged and the undamaged material, respectively. When the stress in an element reaches its failure criteria (Eqs. (13 and 14)) the damage variable is described as

$$D = \begin{cases} 0 & \varepsilon_{t0} \leq \varepsilon \\ 1 - \frac{\sigma'_{tr}}{E_0 \varepsilon} & \varepsilon_{tu} \leq \varepsilon < \varepsilon_0 \\ 1 & \varepsilon \leq \varepsilon_{tu} \end{cases} \quad (16)$$

where σ'_{tr} is the residual tensile strength and ε is the tensile strain of the element.

It is well known that the acoustic emission (AE) can emit due to the micro-fractures or voids occurring frequently inside the soil when the soil is subjected to the internal hydraulic fracture and the surrounding loading. Accordingly, the damage degree of soil can be expressed by the AE number and amplitude, which is

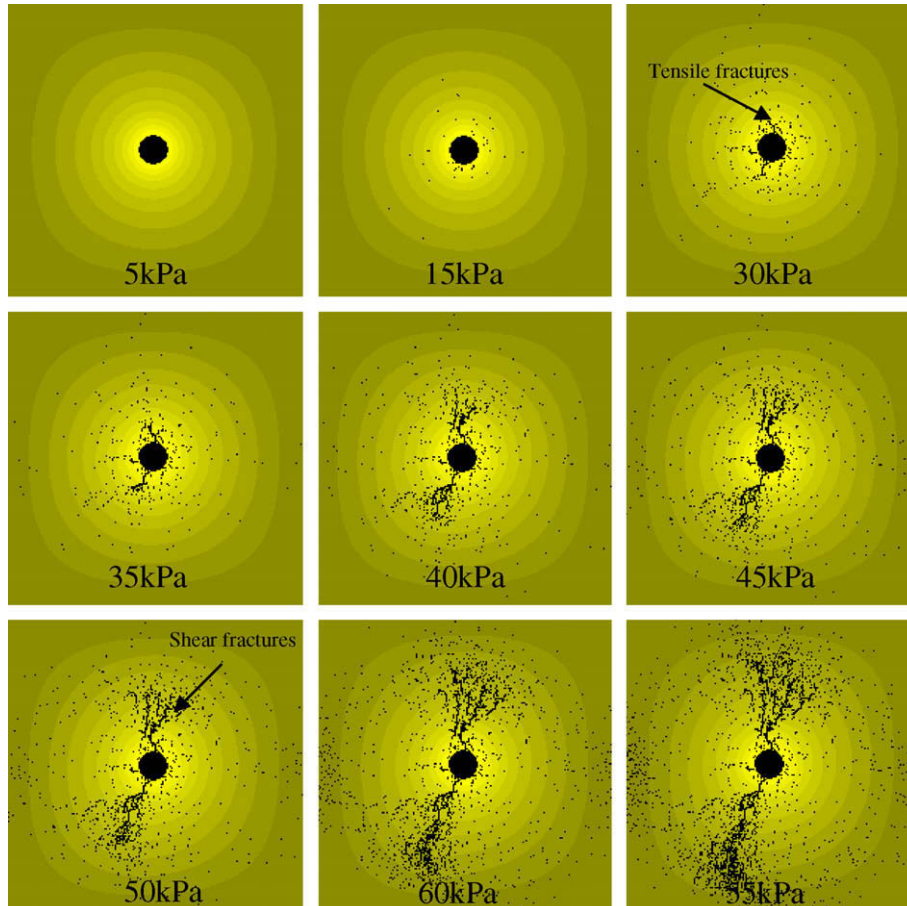


Fig. 6. Numerical simulated hydraulic fractures process ($K_0 = 1, m = 3$).

related with the micro-hydraulic hydraulic fracture evolution inside the stiff soil. In this paper, it is supposed that every fractured element could produce a certain amount of AE when it failed [23]. In this numerical model, hydraulic fracturing produces typically an AE signature as shown in Fig. 4. It is illustrated that the first burst of AE with the injection pressure increased gradually. The first burst is accompanied with opening of the hydraulically induced crack. The magnitude of the pressure at the end of the first burst is regarded as the opening pressure. Furthermore, the AE count rates remain constant after the first burst, and the injection pressure shows the peak and became constant. The crack should be kept open during this time when the injection pressure keeps constant. When the injection is stopped, the injection pressure starts to decrease. Accordingly, the AE count rates starts to increase accompanied with the crack closing. The detailed study of the hydraulic fractures and the associated AE distribution will be carried out in the next sections.

3.2. Model setups

In this paper, the results of three sets of simulations are reported. The first set of simulations is performed to simulate the behavior of stiff clay in the vicinity of an expanding cavity due to the internal hydraulic pressure. The purpose is to develop a better understanding of the crack initiation and propagation mechanisms. In the second set of simulations, the effect of different K_0 on the hydraulic fractures propagation in stiff clay is studied. Meanwhile, the effect of injection rate for the same K_0 is studied. In the third set of simulations, the influence of the heterogeneity of soils on the hydraulic fractures propagation is investigated.

In all of the sets of simulations, the domain is discretized into many small square elements. Coupled seepage and stress analyses are performed. Injection pressure is applied in a quasi-static manner. At each loading increment, the seepage and stress equations of the elements are solved and the coupling analysis is performed. The stress conditions of each element are then examined for failure before the next load increment. Input parameters for these simulations are tabulated in Table 1. The 2-dimensional plane strain numerical model is shown in Fig. 5. The $2\text{ m} \times 2\text{ m}$ domain of analysis was divided into 40,000 elements of material properties following the Weibull statistical distribution depicted in Eq. (12). The value K_0 is defined as the initial stresses ratio of σ'_h/σ'_v . σ_h and σ_v are imposed as boundary conditions. The initial diameter of the cavity was 450 mm. The injection pressure in the cavity is increased in steps of 1 kPa to initiate and propagate cracks around the injection cavity.

4. Numerical simulated results

4.1. Crack initiation and propagation around an injection cavity and the associated AE characteristics

Fig. 6 showed the numerical simulated hydraulic fractures process with K_0 of 1. The injection pressure increased from 0 kPa to 60 kPa, and then stopped the injection. Fig. 7 represents the numerical simulated space distribution of AE due to hydraulic fractures initiation and propagation. From Fig. 6, when the injection pressure was 5 kPa, no fractures occurred around the injection cavity. When the injection pressure increased upto 15 kPa, the

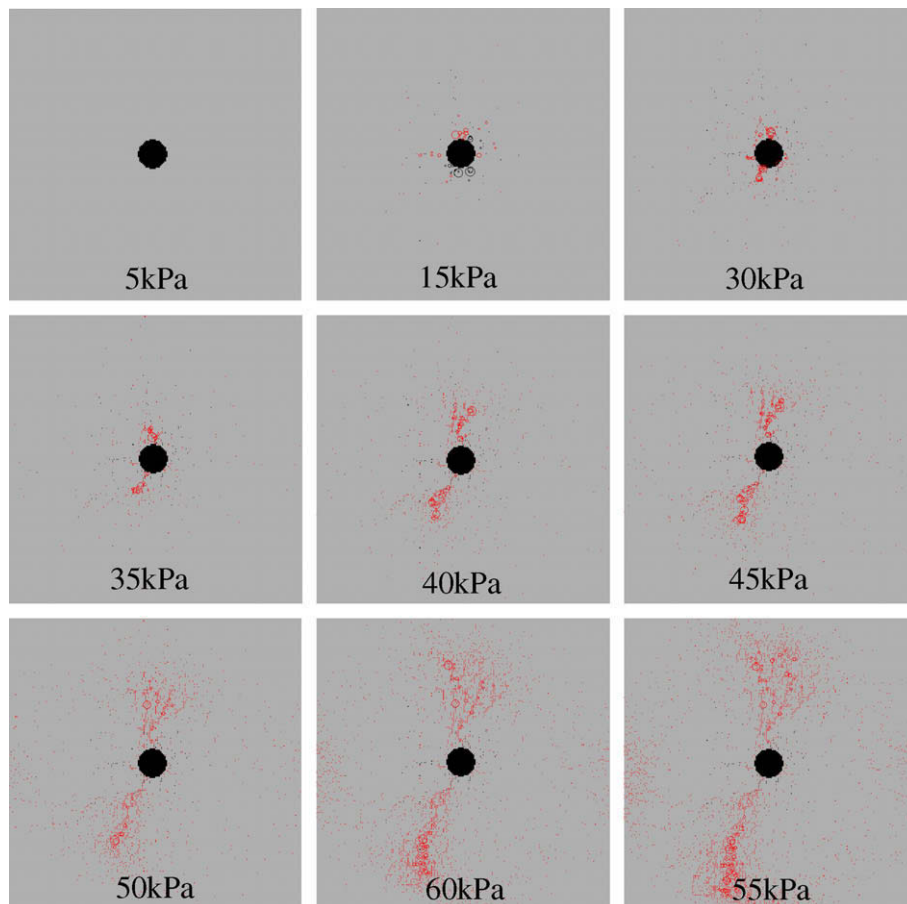


Fig. 7. Numerical simulated acoustic emission (AE) distribution due to hydraulic fractures ($K_0 = 1$, $m = 3$).

micro-crack was initiated. More and more micro-cracks kept on forming when the injection pressure rose to 30 kPa. At this stage, the micro tensile fractures almost distributed homogeneously from the injection cavity, as the K_0 was 1, which meant that only the injection pressure decided the initiation and propagation of micro-fractures. These phenomena can also be verified from the AE distribution in Fig. 7. However, with the injection pressure continuing to increase to 40–50 kPa, the micro-fractures started to interact and coalescence into the several bigger shear fractures. Although both the horizontal and vertical big fractures occurred, most of the big fractures formed in the orientation of 15° symmetrically to the vertical axial.

The entire process of hydraulic fracturing can be divided into four major stages according to the evolution of stress field. (1) Stress concentration stage. During the initial increase of the injection pressure, the stresses increase in the soil with the cavity expanding. There are no new cracks initiated around the borehole (see Fig. 6, injection pressure = 5 kPa). (2) Induced fracture initiation stage. The fractures induced by hydraulic pressure initiate at almost horizontal and vertical direction (see Fig. 6, injection pressure ranging from 5 kPa to 30 kPa). (3) Fracture stable propagation stage. The induced fractures stably propagate under the gradual increase of the hydraulic pressure (see Fig. 6, injection pressure ranging from 30 kPa to 60 kPa). (4) Fracture closing stage. The fractures start to close due the stop of injection.

In addition, when the injection pressure increased 60 kPa, the injection was stopped. The injection pressure started to decreased gradually. In this stage some fractures were closed, however some AE occurred, which could be seen in Fig. 7. Fig. 8 showed the relation of AE counts and energy versus elapsed time. From Fig. 8, the AE counts and energy increased from 0 s to 60 s and reached the

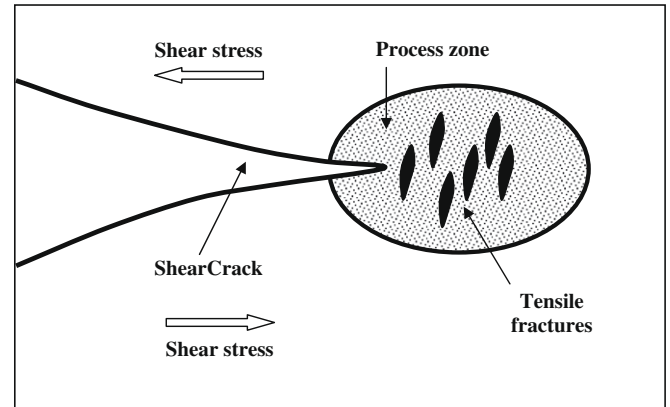
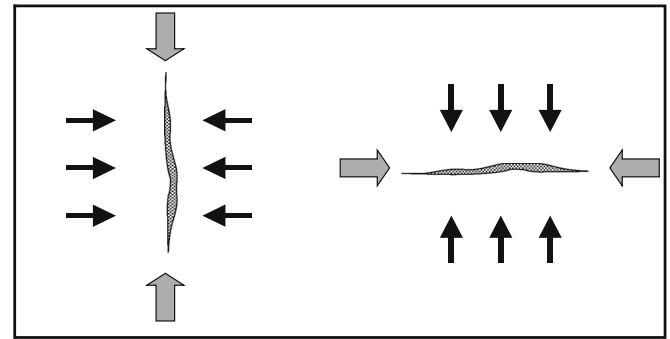


Fig. 10. Illustration of the process zone in which mode I micro-cracking precedes mode II macro-cracking.



(a) $K_0 < 1$ Vertical fracture
(b) $K_0 > 1$ Horizontal fracture

Fig. 11. Schematic fracture propagation directions for different K_0 [9].

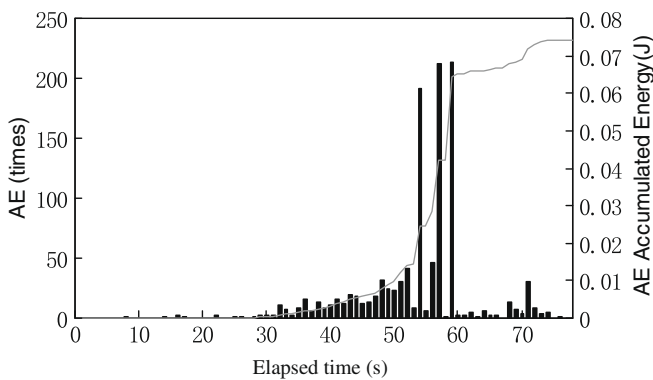


Fig. 8. Numerical simulated AE counts due to micro-cracks in soil specimens with hydraulic pressure increasing (F-RFPA).

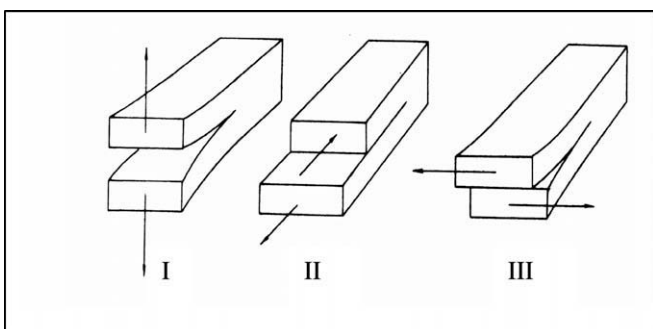


Fig. 9. Diagram showing the three modes of cracking [35].



Fig. 12. Vertical fracture created by low injection rate test [9].



Fig. 13. Horizontal fracture created by high injection rate test [9].

time when the injection pressure kept constant. When the injection was stopped, the injection pressure started to decrease. Accordingly, the AE count rates started to increase accompanied with the crack closing.

As mentioned in Section 2, crack initiation in geo-materials was considered to be either a tensile failure or shear failure in the material. However, what is the relationship of tensile crack and shear crack during the process of hydraulic fractures? Basically there are three crack modes (I, II and III). Mode I is the tensile crack, mode II is the shear crack and mode III is the combined crack. They are illustrated in Fig. 9.

Mode I corresponds to the case of tensional cracking considered up to this point. In fact, it was the most useful mode to study, as experimental evidence [25] showed that even a crack which was, on a macroscopic scale, a mode II crack, actually proceeded by an incremental process of aligned mode I cracking [26]. This was illustrated in Fig. 10. The area ahead of the crack tip is termed the process zone. Some researchers have used cohesive crack model to study the micro-cracked process zone ahead of macro-cracks [27,28]. Within this process zone, the material might be deformed by tensional cracking, which become more intense as the loading increases. Eventually, these micro-cracks link, and the macro-cracks extend. This process had been numerically simulated in Fig. 6. With the increase of injection pressure, failure mechanism

peak value at 60 s. After that the AE count rates decreased abruptly and remained constant. The crack should be kept open during this

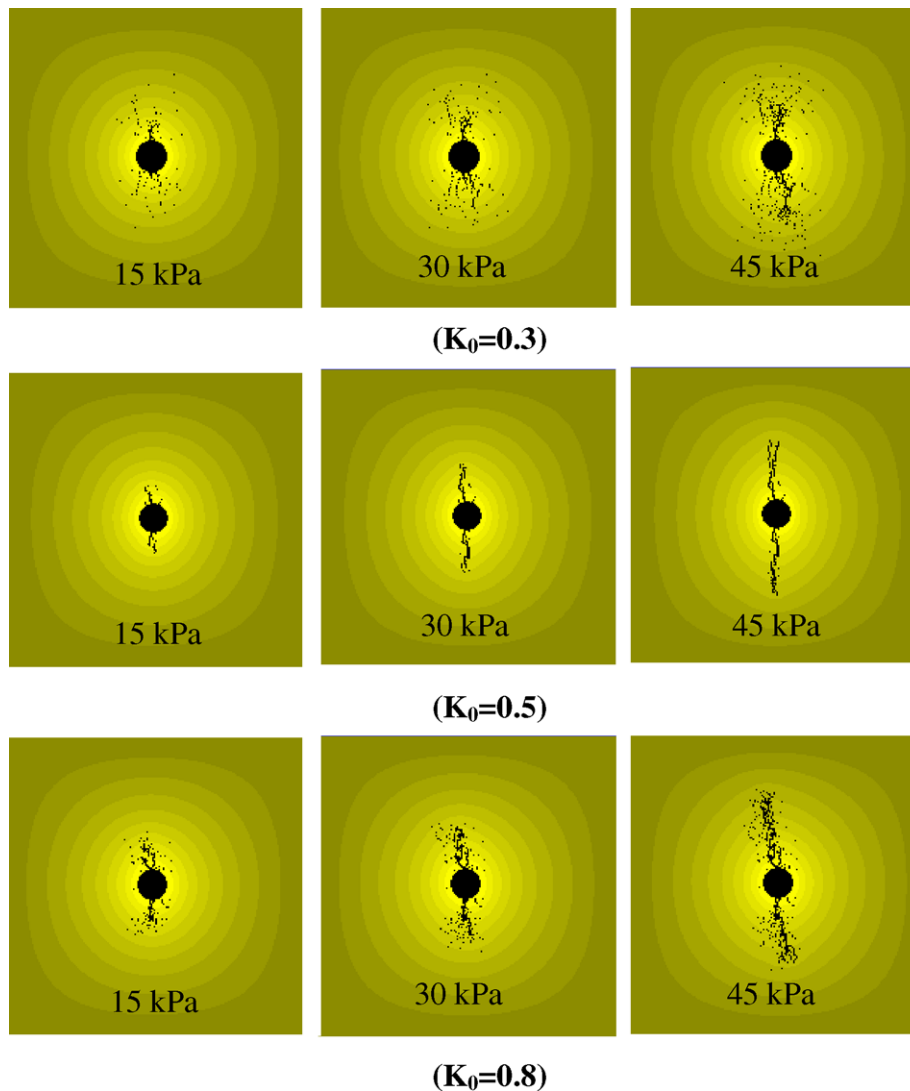


Fig. 14. Numerical simulated hydraulic fractures process when $K_0 < 1$.

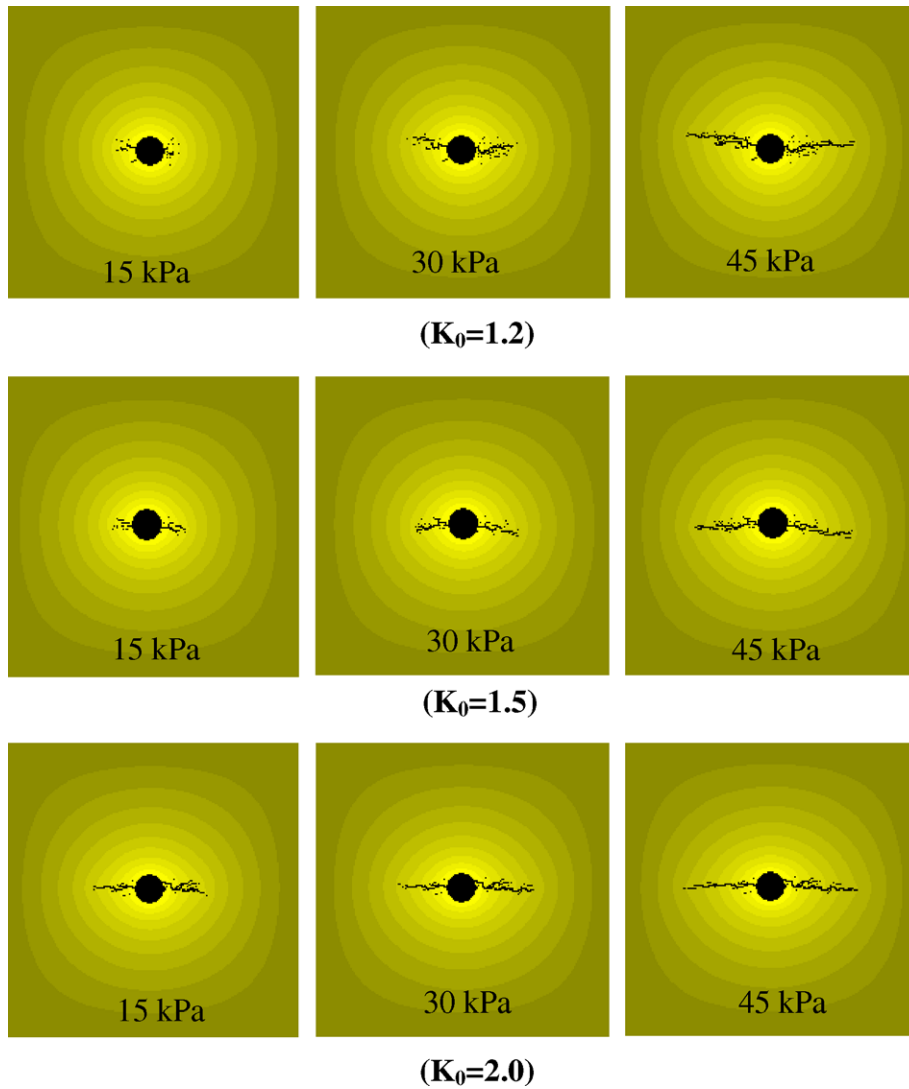


Fig. 15. Numerical simulated hydraulic fractures process when $K_0 > 1$.

will be a tensile failure enhanced by the excess pore water pressure generated by shearing of soil, which resulted from the stress differential between radial stress and circumference stress. For example, from Fig. 6, when the injection pressure was 50 kPa, four shear cracks occurred and there were many small tensile fractures around the tip of each shear cracks. Furthermore, the small tensile fractures interacted and linked to the bigger fractures. Therefore,

the mechanism was in fact a combination of the tensile and shear failure mode.

4.2. influence of lateral pressure coefficient (K_0) on hydraulic fracture

Some researchers [29] considered horizontal and vertical fractures would occur when $K_0 > 1$ and $K_0 < 1$, respectively, as shown

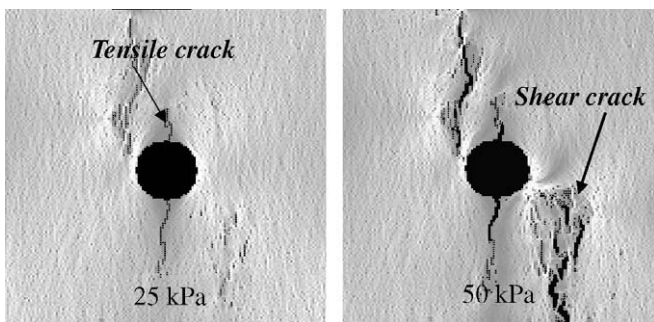


Fig. 16. Evolution of cracks around cavity with low injection rate ($K_0 = 0.6$).

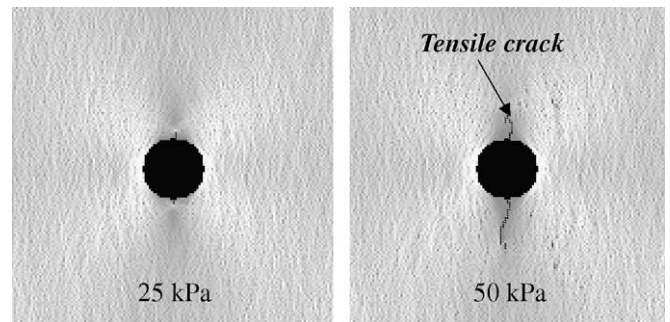


Fig. 17. Evolution of cracks around cavity with high injection rate ($K_0 = 0.6$).

in Fig. 11. However, Lefebvre et al. [30] thought that vertical fracture could be formed even when $K_0 > 1$. Furthermore, Massarsch [31] opined that cracks would be likely to occur along vertical planes during hydraulic fracturing tests in clay, independently of the coefficient of lateral earth pressure, K_0 .

In addition, some researchers [32,33] had considered the soil material properties as an important factor influencing the hydraulic

fracturing. Au [9] suggested that the directions of principal stresses might rotate during the injection process although such rotations might depend on the initial stress conditions. In addition, the fracture propagation was dependent on the injection rate and K_0 of soil. Figs. 12 and 13 show the vertical and horizontal fracture with low and high injection rates in soils for $K_0 < 1$, respectively. It is thus very difficult to study the crack initiation and propagation

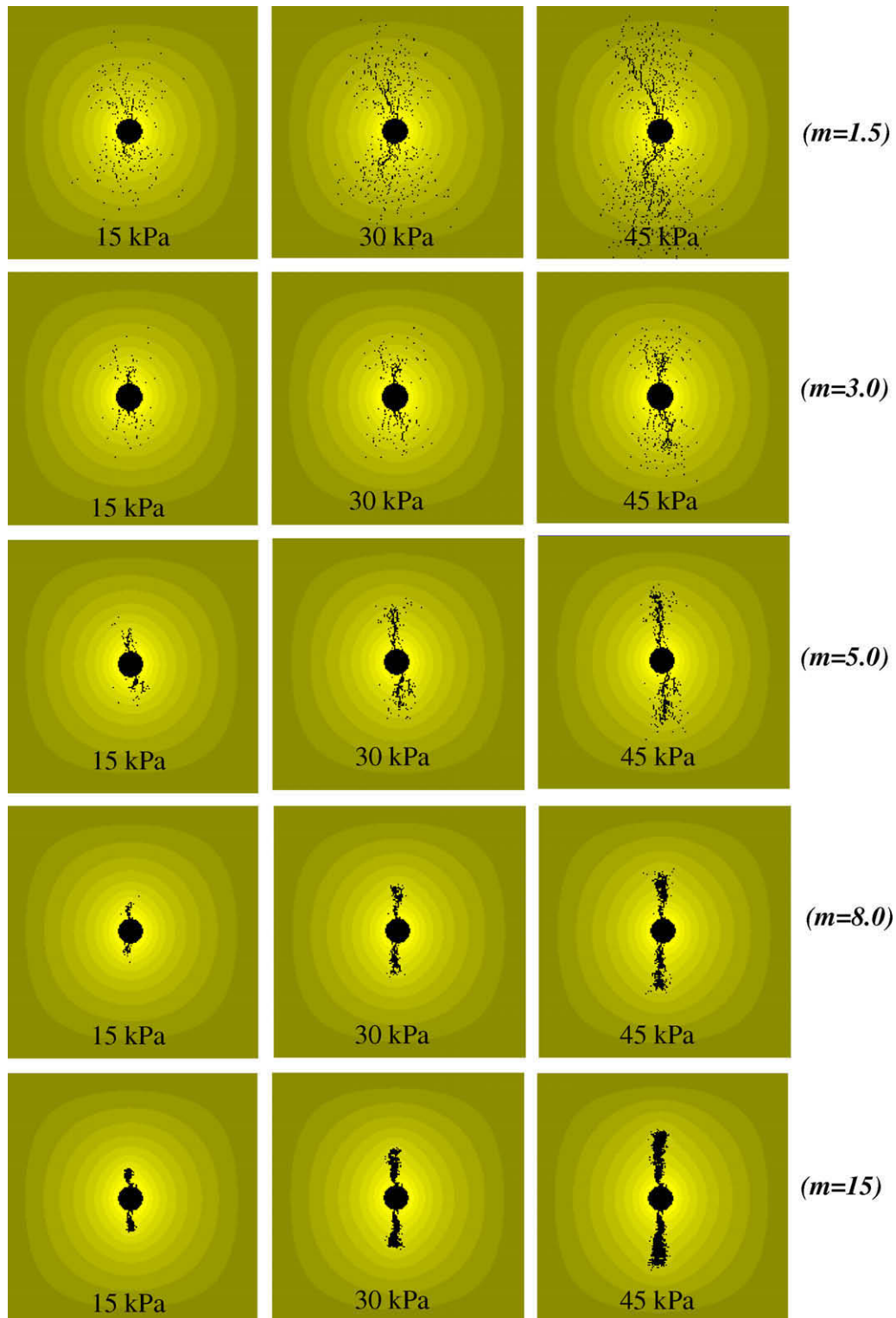


Fig. 18. Numerical simulated hydraulic fractures process for different homogeneity index (m).

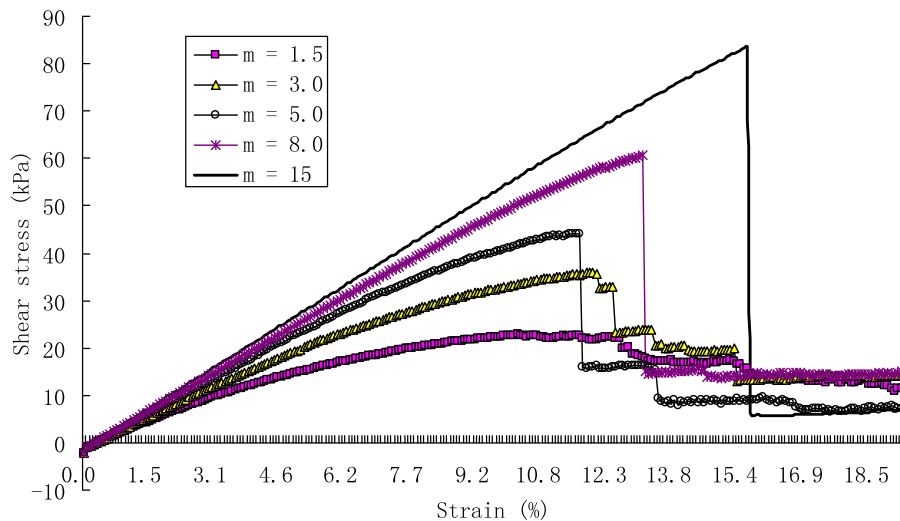


Fig. 19. Influence of material heterogeneity on the stress-strain curves for five specimens with different homogeneity indices.

processes in soil during grouting thoroughly by experiments due to the heterogeneity of soil and the complexity of boundary conditions. Therefore, numerical simulations are used in this investigation.

Fig. 14 shows the numerical simulated hydraulic fractures process when K_0 was 0.3, 0.5 and 0.8, respectively. Fig. 15 showed the numerical simulated hydraulic fractures process when K_0 was 1.2, 1.5 and 2.0, respectively. From Fig. 14, the vertical fractures occurred when $K_0 < 1$. In comparison, the horizontal fractures occurred when $K_0 > 1$. Both the vertical and horizontal fracture initiated and propagated at approximately perpendicular to the direction of the minor principal stress. It is interesting to notice that when $K_0 = 0.8$, the fractures propagated in the direction of about 10° to the vertical direction. That is because the directions of principal stresses might rotate during the injection process. Similarly, when $K_0 = 1.2$ and 1.5, the fractures did not propagate totally following the horizontal direction.

Another factor to affect the hydraulic fractures initiation and propagation is the injection rate (increment of injection pressure/time). Figs. 16 and 17 show the evolution of fractures around cavity with low and high injection rate, respectively, when $K_0 = 0.6$. For the numerical simulation of low injection rate, both tensile cracks and shear cracks were initiated due to the increasing injection pressure. However, the propagation of tensile cracks, i.e., cracks in the vertical direction, stopped at the injection pressure of approximately 25 kPa. However, shear cracks continued to propagate. In this case, both the injection pressure and K_0 condition controlled the initiation of fractures. However, the propagation of fractures was dominated by K_0 for the relative low injection rate. In contrast, for the case of high injection rate in Fig. 19, only the vertical cracks around the cavity initiated and propagated. It indicated that the injection rate dominated the propagation of fractures other than K_0 .

4.3. Influence of heterogeneity of soil on hydraulic fracture

Much stiff clay forming part of slopes and the core section of earth dams exist in the fissured state. These fissures or cracks in the clay can produce stress concentrations that can force the clay beyond its peak strength, producing as a result the non-uniform mobilization of strength, and thus causing the progressive failure of the clay. In this section, soil samples with different homogeneity

index were modeled to study the influence of heterogeneity on the hydraulic fractures process for different homogeneity index ($m = 1.5, 3, 5, 8, 15$). The higher m value represents the more homogeneous of soil. It could be seen from Fig. 15 that, the heterogeneity of soil had an important influence on the fracture propagation pattern. For instance, when $m = 1.5$, many micro-cracks around the injection cavity clustered in the soil with the increasing of hydraulic pressure. However, for much more homogeneous soils ($m = 8$), only few micro-cracks occurred around the injection cavity and a main fracture formed and propagated vertically. In addition, the hydraulic fractures propagated more symmetrically in more homogeneous soil. For instance, for the case of $m = 1.5$, the fractures were not symmetric, however, for the case of $m = 20$, the fractures were almost symmetric. The numerical results indicated the heterogeneity of soil was sensitive to influence the stress field modification when crack occurred, and then influenced the propagation of fractures.

Fig. 19 showed the influence of material heterogeneity on the stress-strain relationships for five specimens with different homogeneity indices ($m = 1.5, 3, 5, 8, 15$). In these five cases, the injection pressure increased gradually with the same injection rate. The stress-strain curves were given by uniaxial loading the specimens. In fact the numerical simulated stress-strain curves in Fig. 19 represented the coupling effect of hydraulic pressure and heterogeneity of soil on the shear strength. From Fig. 19, it was clear that the stress-strain relation and the strength characterization depended strongly on the heterogeneity of the specimen. For the low homogeneous index ($m = 1.5$ or 3), the shape of the strain-strain curves had a gentler post-peak behavior. The peak shear strength of the specimens was also related to the homogeneity index. The higher the value of the homogeneity index, the higher the strength of the specimen. Furthermore, the curves became even linear and the strength loss was also sharper for the more homogeneity specimens.

5. Conclusions

- A geo-material Failure Process Analysis developed for heterogeneous stiff geo-materials coupling stress, seepage and element damage evolution are introduced to investigate the behavior of the crack initiation and propagation in stiff clay during injection.

- Numerical results illustrated that the entire process of hydraulic fracturing can be divided into four major stages: (1) stress concentration stage, (2) induced fracture initiation stage, (3) fracture stable propagation stage and (4) fracture closing stage.
- The concept of process zone is introduced to explain the mechanism of hydraulic fractures propagation is in fact a combination of the tensile and shear failure modes.
- Numerical results reproduced the acoustic emission (AE) characteristic in spatial and time evolution in soils due to the internal hydraulic fracture and the surrounding loading.
- The numerical results indicate K_0 is an important parameter controlling the crack initiation and propagation mechanisms around an injection cavity. Even when $K_0 < 1$, both tensile and shear cracks can develop and propagate. However, the direction of crack propagation could change as the injection pressure increases, resulting in a rotation of directions of principal stresses.
- The propagation of fractures is dominated by K_0 for the relative low injection rate. In contrast, for the case of high injection rate, the injection rate dominates the propagation of fractures other than K_0 .
- The numerical results indicate the heterogeneity of soil is sensitive to influence the stress field modification when hydraulic fractures initiate, and then influenced the propagation of fractures. The higher the value of the homogeneity index, the higher the strength of the specimen. The curves of stress-strain become even linear and the strength loss is also sharper for the more homogeneous specimens.

Acknowledgements

The work described in this paper was partially supported by the National Science Foundation under Grants (CMMI-0408390, CMMI-0644552, 50674025 and 10872046), by the American Chemical Society Petroleum Research Foundation under Grant PRF-44468-G9, by the National Natural Science Foundation of China, by 973 Program of Ministry of Science and Technology of China, by the Australian Research Council under Grant DP0881238, by the Fok Ying Tung Education Foundation, and by the Changjiang Scholarship of Ministry of Education of China, to which the authors are very grateful.

References

- [1] Wong HY, Farmer IW. Hydrofracture mechanisms in rock during pressure grouting. *Rock Mech* 1973;5:21–41.
- [2] Morgenstern NR, Vaughan PR. Some observations on allowable grouting pressures. In: Proc conf grouts and drill muds, Instit Civ Eng, London; 1963. p. 36–42.
- [3] Hubbert MK, Willis DG. Mechanics of hydraulic fracturing. *Trans AIME* 1957;210:153–66.
- [4] Jaworski GW, Duncan JM, Seed HB. Laboratory study of hydraulic fracturing. *J Geotech Eng Div, ASCE* 1981;107(6):713–32.
- [5] Mori A, Tamura M. Hydrofracturing pressure of cohesive soils. *Soils Found* 1987;27(1):14–22.
- [6] Thallak S. Numerical simulation of hydraulic fracturing in granular media. PhD thesis, University of Waterloo, 1991.
- [7] Murdoch LC. Hydraulic fracturing of soil during laboratory experiments: methods and observations. *Geotechnique* 1993;43(2):255–65.
- [8] Andersen KH et al. Estimation of hydraulic fracture pressure in clay. *Can Geotech J* 1994;31:817–28.
- [9] Au SK. Fundamental study of compensation grouting. PhD thesis, Cambridge University, 2001.
- [10] Bjerrum L, Andersen KH. In-situ measurement of lateral pressures in clay. In: European conference on SMFE, Madrid, vol. 1; 1972. p. 11–9.
- [11] Bjerrum L, Nash JKL, Kennard RM, Gibson RE. Hydraulic fracturing in field permeability testing. *Geotechnique* 1972;22(2):319–32.
- [12] Hassani AW, Singh B, Saini SS. Experimental investigation of hydraulic fracturing. *Indian J Power River Valley Dev* 1983;12:181–7.
- [13] Vesic AS. Expansion of cavities in infinite soil mass. *J Soil Mech Found Div, ASCE* 1972;98(3):265–90.
- [14] Carter JP, Booker JR, Yeung SK. Cavity expansion in cohesive frictional soils. *Geotechnique* 1986;36(3):349–53.
- [15] Collins IF, Yu HS. Undrained cavity expansion in critical state soils. *Int J Numer Anal Methods Geomech* 1996;20(7):489–516.
- [16] Chang MF, The CI, Cao LF. Undrained cavity expansion in modified Cam clay II: application to the interpretation of the piezocone test. *Geotechnique* 2001;51(4):335–50.
- [17] Hsieh YM, Whittle AJ, Yu HS. Interpretation of pressuremeter tests in sand using advanced soil model. *J Geotech Geoenviron Eng, ASCE* 2002;128(3):274–8.
- [18] Yanagisawa E, Panah AK. Two dimensional study of hydraulic fracturing criteria in cohesive soil. *Soils Found* 1994;34(1):1–9.
- [19] Decker PA, Clemence SP. Laboratory study of hydraulic fracturing in clay. In: Proceedings of the 10th ICSMFE, Stockholm, vol. 1; 1981. p. 573–5.
- [20] Lo KY, Kaniaru K. Hydraulic fracture in earth and rock fill dams. *Can Geotech J* 1990;27(4):496–506.
- [21] Soga K, Ng MYA, and Gafer K. Soil fractures in grouting. In: Proceedings of the 11th Int'l. Conf computer methods and advances in geomechanics, Torino; 2005. p. 397–406.
- [22] Alfaro MC, Wong RCK. Laboratory studies on fracturing of low permeability soils. *Can Geotech J* 2001;38(2):303–15.
- [23] Tang CA, Tham LG, Lee PKK, Yang TH, Li LC. Coupled analysis of flow, stress and damage (FSD) in rock failure. *Int J Rock Mech Min Sci* 2002;39(4):477–89.
- [24] Karihaloo BL, Fu D. A damage-based constitutive law for plain concrete tension. *Eur J Mech A/Solids* 1989;8:373–84.
- [25] Petit JP, Barquins M. Can natural faults propagate under mode II conditions? *Tectonics* 1988;7:1243–56.
- [26] Cox SJD, Scholz CH. Rupture initiation in shear fracture of rocks: an experimental study. *J Geophys Res* 1988;93:3307–20.
- [27] Xiao QZ, Karihaloo BL. Asymptotic fields at frictionless and frictional cohesive crack tips in quasi-brittle materials. *J Mech Mater Struct* 2006;1:881–910.
- [28] Karihaloo BL, Xiao QZ. Asymptotic fields at the tip of a cohesive crack. *Int J Fract* 2008;150:55–74.
- [29] Essler RD, Droff ER, Falk E. Compensation grouting: concept, theory and practice. In: Krizek RJ, Sharp K, editors. *Advances in grouting and ground modification*. Reston, Virginia: ASCE; 2000. p. 1–15 [Geotech spec publ no. 104].
- [30] Lefebvre G, Bozozuk M, Philibert A, Hornych P. Evaluating K_0 in Champlain clays with hydraulic fracture tests. *Can Geotech J* 1991;28(3):365–77.
- [31] Massarsch KR. New aspects of soil fracturing in clay. *J Geotech Eng Div, ASCE* 1978;104(8):1109–23.
- [32] Erdogan F, Biricikoglu V. Two bonded half planes with a crack going through the interface. *Int J Eng Sci* 1973;11(7):745–66.
- [33] Hanson ME, Anderson GD, Shaffer RJ. Theoretical and experimental research on hydraulic fracturing. *J Energy Resour Technol Trans ASME* 1980;102(2):92–8.
- [34] Mitchell JK, Soga K. *Fundamentals of soil behavior*. 3rd ed. New York: John Wiley and Sons; 2005.
- [35] Lemaitre J, Chaboche JL. *Mécanique Des Matériaux Solides*. Dunod, Paris. [Mechanics of solid materials]. Berlin: Springer Verlag; 1985.